ARMY RESEARCH LABORATORY

Strength-to-Weight Optimization of Titanium Pyramidal Core Sandwich Plates

by Jason R. Tice, Kevin J. Doherty, and Marc Zupan

ARL-RP-182 **June 2007**

A reprint from the *SAMPE 2007 Conference Proceedings*,
Baltimore, MD, 3–7 June 2007.

NOTICES

Disclaimers

The findings in this report are not to be construed as an official Department of the Army position unless so designated by other authorized documents.

Citation of manufacturer's or trade names does not constitute an official endorsement or approval of the use thereof.

Destroy this report when it is no longer needed. Do not return it to the originator.

Army Research Laboratory
Aberdeen Proving Ground, MD 21005-5069

ARL-RP-182 **June 2007**

Strength-to-Weight Optimization of Titanium Pyramidal Core Sandwich Plates

Jason R. Tice, Kevin J. Doherty, and Marc Zupan
Weapons and Materials Research Directorate, ARL

A reprint from the *SAMPE 2007 Conference Proceedings*, Baltimore, MD, 3–7 June 2007.

REPORT DOCUMENTATION PAGE

Form Approved
OMB No. 0704-0188

1. REPORT DATE *(DD-MM-YYYY)*	2. REPORT TYPE	3. DATES COVERED (From - To)
June 2007	Reprint	August 2005–August 2006

4. TITLE AND SUBTITLE
Strength-to-Weight Optimization of Titanium Pyramidal Core Sandwich Plates

5a. CONTRACT NUMBER
ORISE 7263185

5b. GRANT NUMBER

5c. PROGRAM ELEMENT NUMBER

6. AUTHOR(S)
Jason R. Tice, Kevin J. Doherty, and Marc Zupan

5d. PROJECT NUMBER
622105.AH84

5e. TASK NUMBER

5f. WORK UNIT NUMBER

7. PERFORMING ORGANIZATION NAME(S) AND ADDRESS(ES)
U.S. Army Research Laboratory
ATTN: AMSRD-ARL-WM-MD
Aberdeen Proving Ground, MD 21005-5069

8. PERFORMING ORGANIZATION REPORT NUMBER
ARL-RP-182

9. SPONSORING/MONITORING AGENCY NAME(S) AND ADDRESS(ES)

10. SPONSOR/MONITOR'S ACRONYM(S)

11. SPONSOR/MONITOR'S REPORT NUMBER(S)

12. DISTRIBUTION/AVAILABILITY STATEMENT
Approved for public release; distribution is unlimited.

13. SUPPLEMENTARY NOTES
A reprint from the *SAMPE 2007 Conference Proceedings*, Baltimore, MD, 3–7 June 2007.

14. ABSTRACT

Future military vehicles demand increasingly mass-efficient structural armor systems to satisfy design requirements of increased mobility and survivability. In order to fully realize lightweight solutions, sandwich plates consisting of monolithic facesheets and a low-density cellular core are targeted as an integral ingredient in these armor systems, providing both structural strength and stiffness via through-the-thickness load-bearing potential. In this study, sandwich plates consisting of thin facesheets and a periodic pyramidal core manufactured entirely from cold-rolled Grade 4 commercially-pure titanium (CP-1) are investigated. A plausible manufacturing route and its corresponding limitations are established, and analytical models for peak strength ($\overline{\sigma}_{peak}$) and effective stiffness ($\overline{E}$) for flatwise compression are presented. In addition, a strength-to-weight optimization technique is implemented, and model calibration experiments are conducted on the as-manufactured optimized plates. From these experiments, the model for $\overline{\sigma}_{peak}$ was found to be a robust and accurate tool for depicting core performance. Although modeling $\overline{E}$ was less successful, probable causes for reduced precision are presented. Also, the as-manufactured titanium plates are verified to be fully optimized from a strength-to-weight standpoint for flatwise compression.

15. SUBJECT TERMS
sandwich structures, materials-cellular, metals-titanium, optimization, pyramidal core, periodic core, sandwich plate

16. SECURITY CLASSIFICATION OF:			17. LIMITATION OF ABSTRACT	18. NUMBER OF PAGES	19a. NAME OF RESPONSIBLE PERSON
a. REPORT	b. ABSTRACT	c. THIS PAGE			Jason R. Tice
UNCLASSIFIED	UNCLASSIFIED	UNCLASSIFIED	UL	24	19b. TELEPHONE NUMBER (*Include area code*) 410-306-4717

STRENGTH-TO-WEIGHT OPTIMIZATION OF TITANIUM PYRAMIDAL CORE SANDWICH PLATES

Jason R. Tice*, Kevin J. Doherty, and Marc Zupan
US Army Research Laboratory, AMSRD-ARL-WM-MD, Survivability Materials Branch,
Aberdeen Proving Ground, Maryland 21005

ABSTRACT

Future military vehicles demand increasingly mass-efficient structural armor systems to satisfy design requirements of increased mobility and survivability. In order to fully realize lightweight solutions, sandwich plates consisting of monolithic facesheets and a low-density cellular core are targeted as an integral ingredient in these armor systems, providing both structural strength and stiffness via through-the-thickness load-bearing potential. In this study, sandwich plates consisting of thin facesheets and a periodic pyramidal core manufactured entirely from cold-rolled Grade 4 commercially-pure titanium (CP-1) are investigated. A plausible manufacturing route and its corresponding limitations are established, and analytical models for peak strength ($\bar{\sigma}_{peak}$) and effective stiffness ($\bar{E}$) for flatwise compression are presented. In addition, a strength-to-weight optimization technique is implemented, and model calibration experiments are conducted on the as-manufactured optimized plates. From these experiments, the model for $\bar{\sigma}_{peak}$ was found to be a robust and accurate tool for depicting core performance. Although modeling $\bar{E}$ was less successful, probable causes for reduced precision are presented. Also, the as-manufactured titanium plates are verified to be fully optimized from a strength-to-weight standpoint for flatwise compression.

KEYWORDS: Sandwich Structures, Materials-Cellular, Metals-Titanium

1. INTRODUCTION

1.1 Next Generation Military Vision It is customary that military vehicles provide ballistic/blast protection via monolithic metallic plates which are neither weight nor volume efficient. By replacing these thick heavy plates with multifunctional lightweight sandwich panels which provide structural stiffness, strength, and energy absorption, improvements in specific strength, stiffness, and overall survivability can be achieved. In addition, reducing the weight of military vehicles provides benefits including increased range, maneuverability, fuel efficiency, and speed. However, current add-on armor packages tend to improve survivability with increased weight and volume, thus sacrificing size, maneuverability, range, and speed. As the battlefield roles of these advanced vehicles are continuously expanded, they represent excellent platforms for weight reduction through integration of lightweight sandwich plates which provide blast and ballistic resistance as part as an integrated protective package in the vehicle superstructure.

1.2 Topology and Material Selection Sandwich cores including periodic topologies such as pyramidal core have been used in a variety of weight-critical applications. Historically, a pyramidal-type lattice block structure was manufactured by investment casting from aluminum

* This project was supported in part by an appointment to the Internship/Research Participation Program for the US Army Research Laboratory administered by the Oak Ridge Institute for Science and Education through an agreement between the US Department of Energy and USARL.

alloys doped with silicon. These truss structures fail via brittle fracture due to void congregation and high silicon content at the joints. This is a consequence of restricted flow at the joints during the investment casting process (1, 2). With these cast structures, the broad range of structural properties that the pyramidal core topology offers cannot be fully realized due to catastrophic failure at the joints instead of controlled deformation in the cell ligaments. In addition, manufacturing limitations related to these investment cast structures severely limit the ability to rapidly modify and optimize design parameters.

In order to produce a cellular core which demonstrates increased ductility versus cast structures, Zupan, Wadley, and colleagues developed a manufacturing process of die-punching, bending, and transient-liquid-phase (TLP) bonding (3, 4, 5). This process has been applied primarily to low-carbon and stainless steels as well as wrought aluminum alloys to produce an array of core topologies (3, 4). However, the ability to manufacture and model pyramidal core sandwich structures out of a lightweight, high strength, high stiffness material such as titanium has not yet been visited to date.

The focus of this work is to first outline a method for fabricating pyramidal core sandwich plates out of wrought titanium. Then, analytical models depicting through-thickness strength and stiffness will be developed, and a strength-to-weight optimization technique will be implemented. Finally, the optimized core will be manufactured and tested such that the models can be validated. Results from this study will enable pyramidal core sandwich plates to be designed and manufactured for future advanced vehicle applications based on specific design criteria.

2. MATERIAL CONSIDERATIONS

2.1 Manufacturing Route The following steps outline the process for constructing pyramidal core sandwich plates for this study:

1. Sheet material is perforated with a diamond pattern
2. Perforated sheet is cold-formed into the desired three-dimensional corrugated core
3. Core and facesheet components are joined via active brazing processes

This process may be used to manufacture pyramidal core sandwich plates out of a variety of sheet materials with some specific limitations which will be detailed as they become apparent.

2.1.1 Sheet Perforation The periodic three-dimensional pyramidal core geometry is created in two steps. First, a computer-numerically-controlled (CNC) abrasive water-jet is utilized to perforate the desired diamond pattern into titanium sheet material. A perforated sheet of CP-1 can be viewed in Figure 1, displaying all pertinent geometric design parameters and the naturally-occurring fold lines.

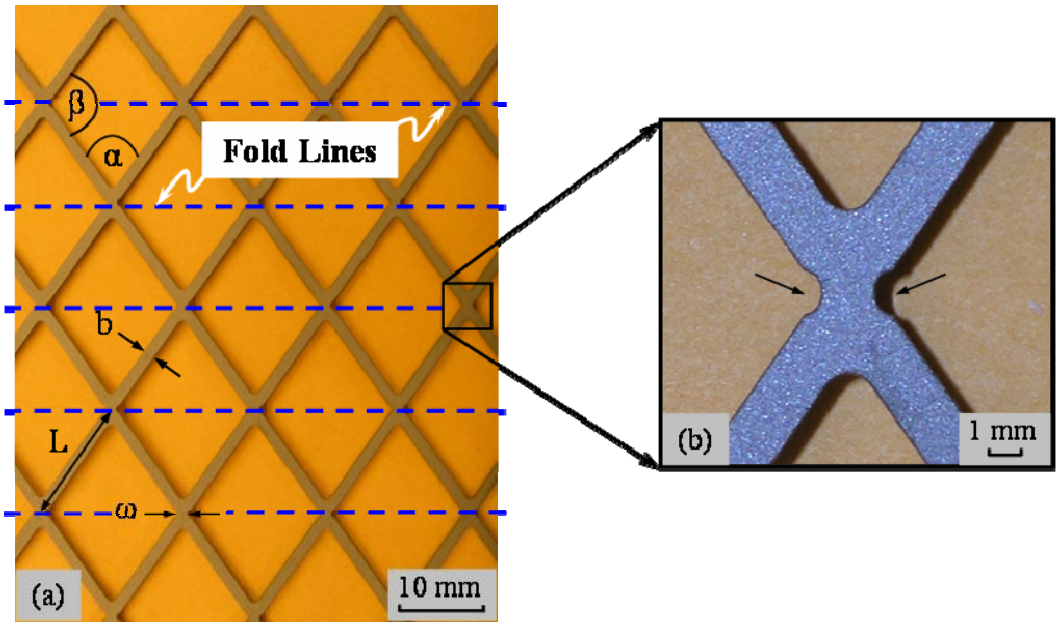

Figure 1: (a) Titanium sheet material is perforated with abrasive water-jet technology with (b) notches machined along the fold lines to improve bend repeatability

In Figure 1(a), geometric parameters for the perforated sheet are shown, where α and β are the minor and major angles in each diamond respectively, b is strut width, L is strut length, and ω is the width of the strut intersection across which bending will occur. The bend lines for this design are naturally occurring at the intersection of the cell ligaments, or struts. Although a rolling punch and die configuration could produce similar perforated sheets for most materials (4), the use of a CNC abrasive water-jet allows design changes to occur quickly. In addition, implanting small notches in the root of the perforated sheet design; Figure 1(b); improves the repeatability of the bending process, resulting in a more consistent panel geometry and improved adhesion of the core and facesheet components. These notches enhance formability of the sheet by reducing material along the bend axis, thereby providing free surfaces for strain relief during cold-forming.

Limitations in manufacturing play an essential role in material selection and core design. The most important limitation associated with water-jet perforation of sheet material involves scaling down the design. There is difficulty achieving consistent strut widths of less than 2 mm because of restricted machine precision and excessive sheet vibration during cutting. This limitation results in a flat strut cross-section which does not adversely affect core design because increasingly slender struts are required for symmetric buckling to occur.

2.1.2 Core Fabrication The second step in fabricating a pyramidal core entails bending the perforated sheet using a hydraulic press-brake forming machine. The perforated sheet is bent using a displacement-controlled punch and an air die; Figure 2. The perforated sheet is then placed in a three-point loading configuration, where it is turned over after each successive bend, resulting in a corrugated pyramidal core; Figure 2(b).

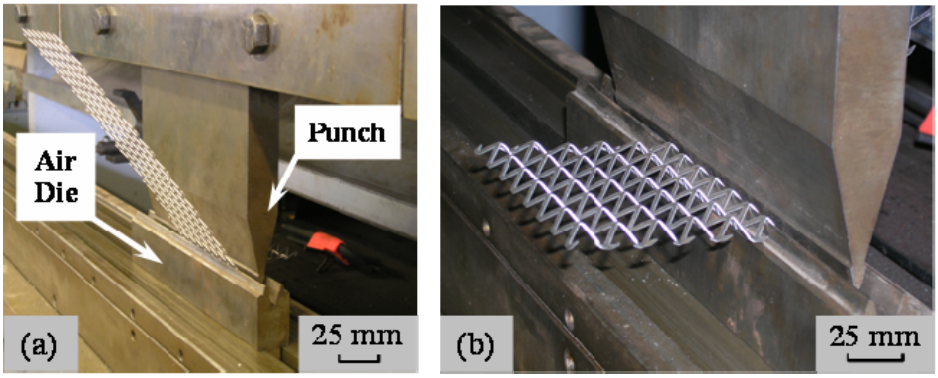

Figure 2: The bending process consists of (a) bending the perforated sheet back and forth multiple times, forming (b) the desired pyramidal core geometry

The resulting product is a periodic three-dimensional array of pyramidal unit cells; Figure 3.

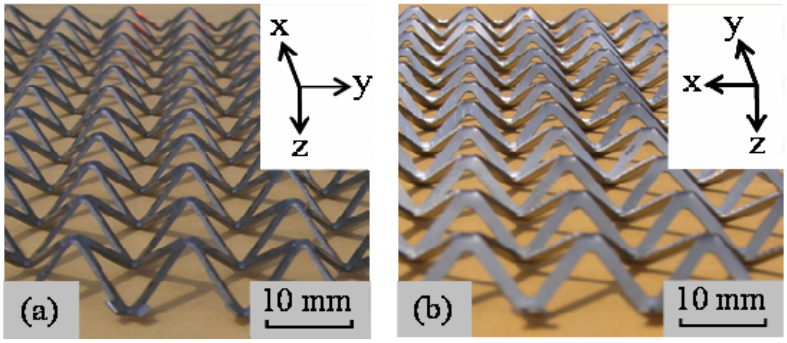

Figure 3: A periodic array of pyramidal cells (a) parallel to the bend axis and (b) perpendicular to the bend axis

A schematic of the salient dimensions of a pyramidal core quarter unit cell is displayed for the reader's convenience in Figure 5. Here, H is pyramid height, X and Y are the base dimensions, L is strut length, b is strut width, t is strut thickness, Φ is bend angle, and θ is the interior angle between the struts and base. These parameters completely depict the core topology for modeling and design purposes.

This bending procedure imposes a number of limitations on the design of pyramidal core structures. The most important limitation imposed by bending is material selection. Material alloy and thickness must be selected based on its ability to be formed to the desired geometry. For thin ductile sheet materials, die spacing should be minimized to achieve sharp bends. For thicker less ductile sheet materials, die spacing should be increased, resulting in bends with increased curvature. In both cases, die spacing limits the distance between neighboring pyramid peaks such that it can never exceed the dimension Y. If spring-back occurs, which is common in titanium, the distance between neighboring pyramid peaks must be a minimum of 20% greater than the die spacing due to the increased displacement required to compensate for spring-back. In addition, punch geometry also limits the perforated sheet thickness that can be formed to the desired bend angle. For CP-1, the bend radius must be 4-5 times that of the sheet thickness in order for it to be cold formed (6). For a punch and die system where punch tip radius is 1.6 mm and die spacing is 13 mm, the resulting bend radius is 2.6 mm. Using this tooling, 0.61 mm thick perforated CP-1 was successfully cold-formed to the desired geometry.

2.1.3 Joining For this study, pyramidal core sandwich plates were constructed from facesheets and the as-manufactured cores via active braze joining techniques. Facesheets of 1.22 mm CP-1 were cut to match core dimensions. Prior to brazing, all components underwent surface treatment to remove all oxides and to ensure uniform surface reactivity, wetting, and flow (7).

Following this surface treatment, a single layer of braze tape (BRAZ1954™) was applied to each facesheet using a steel roller and parts were stacked into the desired sandwich configuration. The arrangement was placed in a vacuum or retort furnace under the appropriate deadweight pressure to minimize drifting of parts during thermal processing. All titanium sandwich plates manufactured in this study were subjected to the optimized thermal treatment as determined by Doherty and Tice et. al. (7). The resulting bonded structure is a periodic pyramidal core sandwich plate with monolithic facesheets, as displayed in Figure 4.

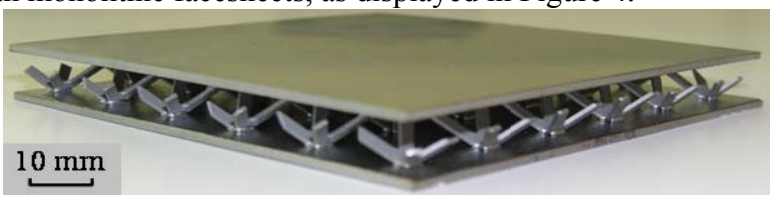

Figure 4: An example titanium pyramidal core sandwich panel (post-brazing)

It is important to note that previous studies have shown joint strength to be vital to core performance because the connectivity provided by the facesheets is required to invoke the stretch-dominated deformation exhibited by the pyramidal core topology (7).

2.2 Analytical Modeling For this study, pyramidal core performance is characterized by peak collapse strength and effective stiffness for out-of-plane compression. Analytical models for these core properties are cast so that they can be calibrated with explicit experimental measurements. These models provide useful insight for design and optimization purposes.

For the pyramidal core geometry displayed in Figure 4, micromechanical models for strength and stiffness are developed by analyzing a quarter unit cell; Figure 5.

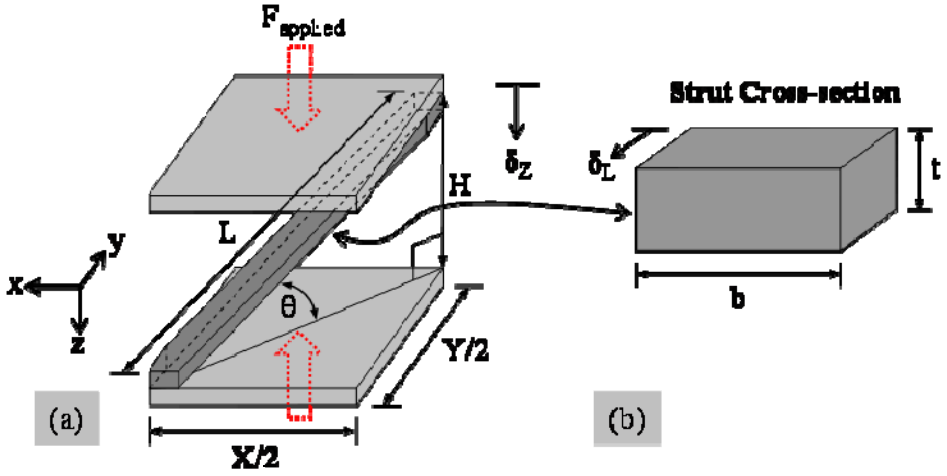

Figure 5: A quarter core and facesheet model is used to analyze the pyramidal core topology because of its four-fold rotational symmetry about the z-axis

In Figure 5(a), a quarter pyramid is displayed and interior angle θ, strut length L, and core height H, are defined. Figure 5(b) shows strut cross-sectional dimensions, thickness t and width b, both of which are measured perpendicular to the strut length. For a complete unit cell where θ is equal for all struts, the pyramidal geometry has four-fold rotational symmetry about the z-axis. Thus, the quarter model can be scaled up by a factor of 4 to depict a complete unit cell.

2.2.1 Peak Strength Model An analytical description of flatwise peak collapse strength exhibited by pyramidal core is obtained through a force resolution assuming static equilibrium in the z-direction. Facesheets are assumed to be sufficiently thick and intimately bonded to the core such that all external loading is transferred into axial loading of the struts. Facesheets also provide adequate connectivity to prevent lateral movement of the joints in the x-y plane ($\delta_x = \delta_y = 0$). Strut geometry is assumed to be sufficiently wide and thin (b/t>2), resulting in a natural buckling plane parallel to the strut width as well as negligible torsional deformation. Considering these assumptions, the force applied to the system, $F_{applied}$, is resolved directly into the axial load carried by the strut, F_{strut}. For static equilibrium in the z-direction, considering four-fold symmetry, the following result presents itself:

$$F_{applied} = 4 \cdot F_{strut} \cdot \sin(\theta) \quad [1]$$

Treating a unit cell as a monolithic plate, the stress distribution within the control volume can be written as a function of total applied load:

$$F_{applied} = \bar{\sigma} \cdot X \cdot Y \quad [2]$$

where $\bar{\sigma}$ is the applied or nominal core stress.

For a square-based pyramid imposed by core symmetry, base dimensions X and Y are:

$$X = Y = \frac{2 \cdot H}{\sqrt{2} \cdot \tan(\theta)} \quad [3]$$

Also, the axial force carried by a single strut can be written in terms internal strut stress:

$$F_{strut} = \sigma_{strut} \cdot A_{strut} = \sigma_{strut} \cdot b \cdot t \quad [4]$$

Substituting $F_{applied}$ and F_{strut} into the equilibrium balance and solving for nominal stress gives:

$$\bar{\sigma} = \frac{2 \cdot b \cdot t}{H^2} \cdot \frac{\sin^3(\theta)}{\cos^2(\theta)} \cdot \sigma_{strut} \quad [5]$$

This result indicates that peak collapse strength $\bar{\sigma}_{peak}$ for pyramidal core can be determined by establishing the initiation of strut failure. Because of symmetry, it is assumed that all struts carry equal load and exhibit identical failure mechanisms. If failure occurs when internal strut stress reaches the yield strength σ_y of the parent material, then core strength can be predicted as:

$$\bar{\sigma}_{peak} = \frac{2 \cdot b \cdot t}{H^2} \cdot \frac{\sin^3(\theta)}{\cos^2(\theta)} \cdot \sigma_y \quad [6]$$

Here σ_y is the yield stress of the parent material in the as-processed condition. This assumption of strut failure stress does not account for elastic buckling which may occur at some stress less than σ_y, nor does it account for plastic buckling which may occur at a stress greater than σ_y due the strain hardening behavior exhibited by some metals. In light of these deficiencies, a more definitive characterization of failure stress should be investigated.

A more robust definition of strut collapse stress is determined by evaluating the actual bifurcation stress at the onset of collapse, σ_{bif}. Bifurcation stress is evaluated by the Shanley Tangent Method of determining buckling strength of a slender strut. In this method σ_{bif} is found by iteratively evaluating the tangent modulus E_t along the true stress-strain response of the parent material until the equality is satisfied. Bifurcation stress is determined as follows:

$$\sigma_{bif} = \frac{\pi^2}{12} \cdot \frac{t^2}{\left(\frac{L}{n}\right)^2} \cdot E_t \qquad [7]$$

where t and L are strut thickness and length respectively, and n is the strut end condition. This analysis is valid for both plastic and elastic collapse regimes, and results in an expanded representation of internal strut stress at failure. By using the bifurcation stress as the definition of strut failure in pyramidal core, the following analytical model is ascertained:

$$\overline{\sigma}_{peak} = \frac{2 \cdot b \cdot t}{H^2} \cdot \frac{\sin^3(\theta)}{\cos^2(\theta)} \cdot \sigma_{bif} \qquad [8]$$

where peak collapse strength is given entirely in terms of core geometry and parent material stress-strain response. This micromechanical relationship provides a complete description of core collapse strength for slender strut designs where torsional deformation is negligible.

2.2.2 Effective Stiffness Model An analytical model to describe the out-of-plane compressive stiffness of pyramidal core is ascertained by performing a work-balance on the quarter model presented in Figure 5. Once the possible collapse mechanisms for a definitive strut geometry are identified, a strain distribution satisfying the upper-bound theorem can be defined. Subsequently, the external work added to the system by an applied force, $W_{applied}$, is equated to the internal work dissipated by each strut, W_{strut}, due to micro-stretching of the core topology for the proposed collapse mode. Again, using the quarter model and considering four-fold symmetry, the following work-balance presents itself:

$$W_{applied} = 4 \cdot W_{strut} \qquad [9]$$

From mechanics, work is calculated as:

$$W_{applied} = F_{applied} \cdot \delta_z = \overline{\sigma} \cdot X \cdot Y \cdot \delta_z \qquad [10]$$

$$W_{strut} = F_{strut} \cdot \delta_\theta = \sigma_{strut} \cdot b \cdot t \cdot \delta_\theta \qquad [11]$$

where δ_z and δ_θ are displacements in the z and θ directions respectively; Figure 5. These displacements can then be written in terms of nominal applied stress $\overline{\sigma}$ as follows:

$$\delta_z = \varepsilon_z \cdot H = \frac{\overline{\sigma} \cdot H}{\overline{E}} \qquad [12]$$

$$\delta_\theta = \varepsilon_z \cdot L \cdot \sin(\theta) = \frac{\sigma_{strut} \cdot L \cdot \sin(\theta)}{E_{strut}} \qquad [13]$$

where $\overline{E}$ is the effective compressive stiffness of the pyramidal core, and E_{strut} is the modulus of the parent material (E_{solid}). From geometry, strut length can be written as:

$$L = \frac{H}{\sin(\theta)} \qquad [14]$$

Furthermore, applying the plastic and elastic collapse modes defined in the previous section for the peak strength model, $\bar{\sigma}$ becomes $\bar{\sigma}_{peak}$, and σ_{strut} becomes σ_{bif}. Making all of these substitutions into the original work-balance; equation 9; results in the following equality:

$$\frac{8 \cdot b^2 \cdot t^2}{H} \cdot \frac{\sin^4(\theta)}{\cos^2(\theta)} \cdot \frac{{\sigma_{bif}}^2}{\bar{E}} = \frac{4 \cdot b \cdot t \cdot H}{\sin(\theta)} \cdot \frac{{\sigma_{bif}}^2}{E_{solid}} \qquad [15]$$

where the left side of the equality is the external work done to the core by an applied force and the right side is the internal work dissipated by the core via strut deformation. Solving equation 15 for effective core stiffness results in the following analytical representation:

$$\bar{E} = \frac{2 \cdot b \cdot t}{H^2} \cdot \frac{\sin^5(\theta)}{\cos^2(\theta)} \cdot E_{solid} \qquad [16]$$

This micromechanical model provides an upper-bound description of compressive core stiffness in terms of core geometry and parent material Young's modulus. This model assumes perfectly rigid components, including facesheets and joints (8).

2.3 Strength-to-Weight Optimization Determining a potential optimization technique for maximizing pyramidal core performance is critical to future implementation of this structure into complex weight-efficient systems and vehicles. Since many prospective applications of pyramidal core require superior out-of-plane performance in conjunction with multifunctionality, out-of-plane compressive strength $\bar{\sigma}_{peak}$ has been targeted as the primary attribute for optimization. More specifically, this study focuses on achieving a maximum flatwise compressive strength at a minimum weight design. The following section outlines the optimization technique implemented here and the implications of manufacturing limitations as they are imposed on the design of a pyramidal core topology.

As shown earlier in equation 8, pyramidal core compressive strength is completely dependent on parent material stress-strain behavior and core geometry. For the manufacturing process outlined in 2.1, it has been shown that choice of parent material is limited to those commercially-available materials which can be successfully cold-formed to the desired bend angle Φ. Thus, parent material behavior σ_{bif} and strut thickness t are predetermined during the material selection process. Furthermore, it is assumed that four-fold rotational symmetry will hold true resulting in a square pyramid base. Thus, the core geometric parameters b, θ, and H are potential free variables which can be targeted for optimization.

2.3.1 Design Parameter Limitations In light of the water-jet limitations presented in 2.1, a lower boundary on strut width b is established such that b must be greater than 2 mm for the manufacturing process prescribed in this study. By graphically investigating the effect b has on $\bar{\sigma}_{peak}$ and $\bar{\rho}$, the ideal b is found for a strength-to-weight optimized strut using the relationships established in equations 8 and 16. The corresponding schematic trends of these functions are presented in Figure 6 for typical pyramidal core geometric parameters.

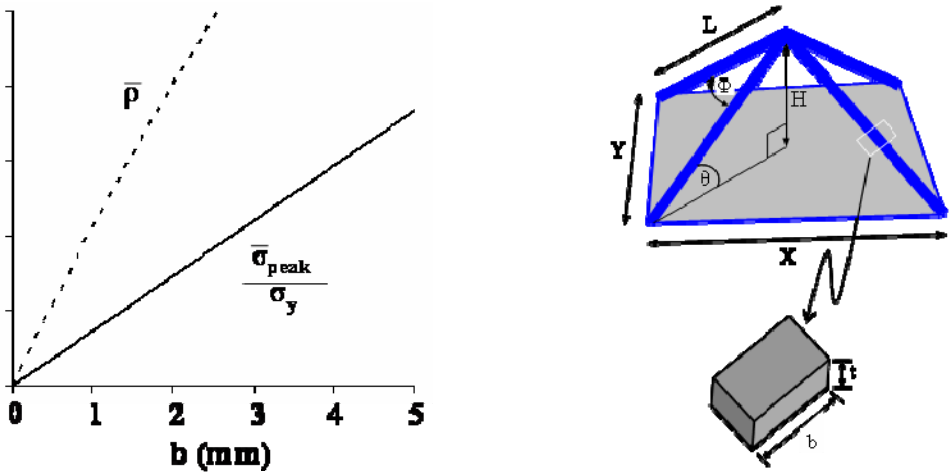

Figure 6: Strut width b has a greater effect on relative density than on strength and thus should be minimized in order to achieve optimal weight efficiency

The relationships offered in Figure 6 show that strut width b has a linear effect on increasing strength and a slightly non-linear effect on $\bar{\rho}$. Since b increases $\bar{\rho}$ at a higher rate than it improves strength, b should be minimized within the manufacturing limitations resulting in maximum core performance from a minimum weight standpoint.

An investigation of interior angle θ as an optimization parameter reveals that punch and die limitations impose a lower bound on the pyramid base dimensions X and Y. Since these dimensions are a function of θ; equation 3; it becomes evident that they impose an upper bound on θ. This results in out-of-plane core strength being maximized as $\theta \to 90°$. Given the relationship between interior angle θ and bend angle Φ:

$$\theta = \arccos\left\{\frac{\sqrt{2}\cdot\tan\left(\frac{\Phi}{2}\right)}{\sqrt{\left[1+2\cdot\tan\left(\frac{\Phi}{2}\right)\right]}}\right\} \qquad [17]$$

core geometry approaches an optimized design as bend angle $\Phi \to 180°$, or a vertical strut. Since this would not correspond to a pyramidal core topology, nor would the core exhibit other attributes not examined in this study, some addition considerations must be made. In light of manufacturing limitations imposed by the tooling used to form the core, the maximum obtainable bend angle Φ is 90° corresponding to an interior angle θ of 35.3°. The optimized parameters b and Φ described here will be used in combination with other constraints to identify the optimal pyramidal core geometry.

2.3.2 Strut Optimization The resulting limitations imposed on b and Φ are important because they establish finite bounds for optimizing pyramidal core performance. Fortunately, pyramid height H is a free variable that is both easily modified and critical to core performance as indicated in equations 8 and 16. Since the height H can be determined in terms of strut length L; equation 14; it becomes immediately evident that $\bar{\sigma}_{peak}$ decreases significantly with increasing L; therefore L is pursued as the primary optimization parameter for this study.

If a basic definition of strut collapse can be established in terms of L, then the optimal L can be determined in order to maximize core performance for a minimum weight design. Since the strength model posed in equation 8 assumes that all loading in the z-direction is distributed along the axis of each strut (θ-direction) and that each strut exhibits a natural buckling plane parallel to strut width b; a basic model of strut collapse can be derived. In Figure 7, the normalized schematic mapping of collapse for elastic and plastic buckling is presented for struts with hinged end supports (n=1).

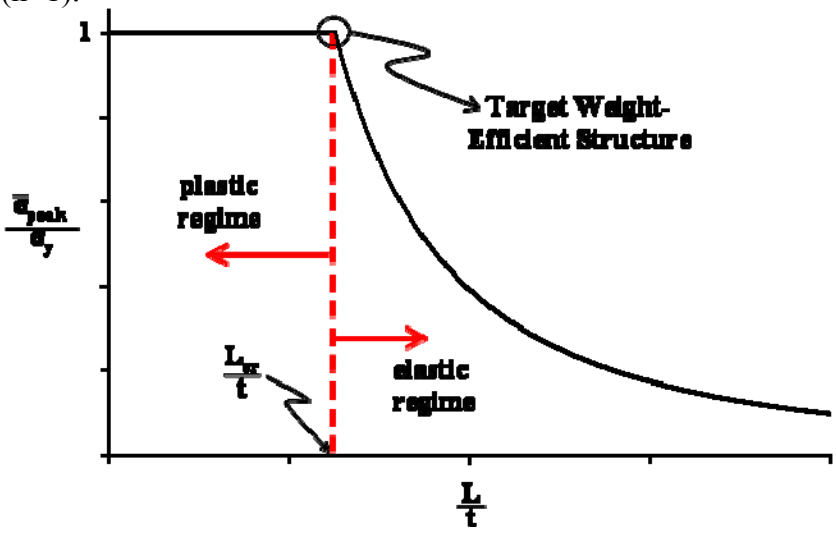

Figure 7: For a slender strut in compression, collapse can occur due to elastic or plastic buckling depending entirely on strut geometry

In Figure 7, plastic buckling occurs at the yield strength of the parent material. A strut designed with this geometry is short or stubby, thus replicating a compression specimen yielding. A strut that undergoes plastic buckling is not weight-efficient because equivalent strength is achievable with a reduced volume of material. Conversely, elastic buckling occurs at a stress level less than the yield strength of the parent material for slender struts. A strut with length $L>L_{cr}$ buckles suddenly due to elastic misalignment of atoms in the microstructure during loading. Failure of this type has been characterized by Euler buckling as follows:

$$P_{cr} = \frac{\pi^2 \cdot n^2 \cdot E_{solid} \cdot I}{L^2} \qquad [18]$$

where P_{cr} is the critical load at which unstable collapse occurs, n is the strut end condition (n=1 for perfectly-pinned ends, n=2 for fully-clamped ends), and I is the second moment of inertia of the strut cross-section. For the rectangular cross-section in this study, $I = \frac{1}{12} \cdot b \cdot t^3$.

Dividing by strut cross-section to determine σ_{cr} and substituting for I, the following relationship for the elastic failure regime of a slender strut is identified:

$$\sigma_{cr} = \frac{\pi^2 \cdot n^2 \cdot E_{solid} \cdot t^2}{12 \cdot L^2} \qquad [19]$$

As displayed in Figure 7, the optimal design space for a slender strut occurs at the intersection of the elastic and plastic buckling regimes. This critical point is the L/t ratio which corresponds to the maximum volume of material in which elastic buckling will occur, or the minimum volume

of material for which plastic buckling will occur. In either case, σ_{cr} is very close to the yield strength of the parent material. Applying this definition of failure stress in equation 19 results in an analytical relationship for optimized strut length:

$$L = \frac{\pi \cdot n \cdot t}{2} \cdot \sqrt{\frac{E_{solid}}{3 \cdot \sigma_y}} \qquad [20]$$

Here, n is found experimentally based on adhesion of the core and facesheet components; thus L is heavily dependent on parent material thickness, modulus, and yield strength.

If a strut is designed to the length as described above, it is guaranteed to fail elastically because of the well-known Perry-Robinson curve. This relationship shows that elastic buckling occurs at a stress below the elastic and plastic regions displayed in Figure 7. Although the optimization technique in this study does not account for this known reduction in collapse stress described by the Perry-Robinson relationship, the guaranteed elastic strut failure that the optimized design exhibits simplifies the buckling mode during compression. This is critical to modeling the performance of the pyramidal core topology. Further work would be required to optimize the strength of a less slender strut geometry because torsional effects would have to be considered.

From this analysis it is evident that there are three key factors in maximizing flatwise compressive strength $\overline{\sigma}_{peak}$ of the pyramidal core topology. First, strut width b should be minimized because of its adverse effect on relative density. Second, bend angle Φ should be maximized in order to orient the majority of core material in the direction of loading. Third, strut length L should be optimized such that strut volume is minimized, but the onset of strut collapse occurs near the yield strength of the parent material.

2.3.3 Optimized Design For the commercially-available core material used in this study (CP-1), t=0.61 mm, E_{solid}=110 GPa and σ_y=600 MPa, in the as-processed condition. In addition, end condition n is estimated to be 1.6 based on inspection of preliminary experiments (7). Utilizing the optimization concepts described previously, all pertinent geometric parameters can be determined for a strength-to-weight optimized pyramidal core. The complete list of optimized design parameters is presented for the reader's convenience in Table 1 of the Appendix.

To conclude the optimization section, it is important to note that all geometric pyramidal core parameters are determined once the parent material alloy and sheet thickness are selected and the optimization technique is implemented. In light of this optimization, one should recognize that there is a fixed optimal relative density that corresponds to the choice of parent material. In this study, the optimal $\overline{\rho}$ for pyramidal core manufactured from 0.61 mm thick CP-1 is 0.04 (7).

3. EXPERIMENTAL

3.1 Procedure for Flatwise Compression Testing In this study, pyramidal core performance is characterized in terms of peak strength and stiffness in flatwise compression. In order to verify the micromechanical models presented in section 2.2, optimized pyramidal core sandwich plates were manufactured as described previously, and uniaxial through-thickness compression testing was conducted conforming to ASTM C365 (9); Figure 8.

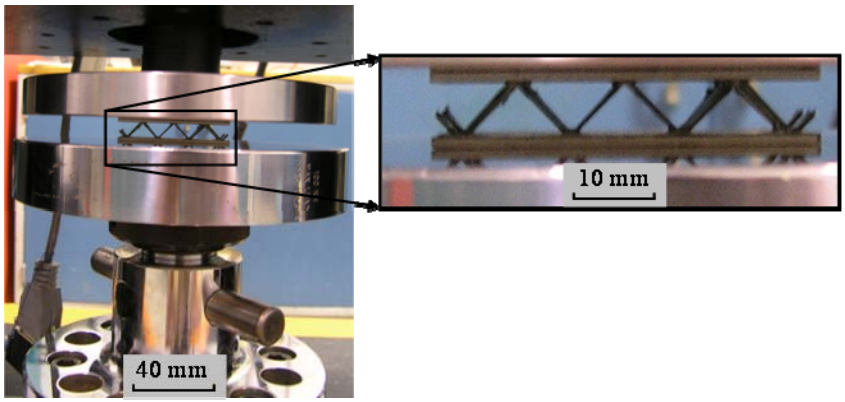

Figure 8: Performance of the optimized pyramidal core sandwich is characterized via flatwise compression under quasi-static loading conditions

For this study, test plates consisted of 4-6 unit cells, and have been shown to exhibit equivalent properties to an infinite sheet. As described previously, facesheets have been chosen sufficiently thick and intimately bonded to the core such that all vertical loading is transferred entirely to the core, with facesheet deformation being elastic and small compared to that of the struts. This ensures that all plastic deformation exhibited by these plates is attributed to the stretch-governed energy dissipation of the core topology (8).

3.2 Compression Results and Discussion The quasi-static ($\dot{\varepsilon} = 10^{-4}$) nominal stress-strain results for flatwise compression of the optimized pyramidal core sandwich plates ($\overline{\rho} = 0.04$) are presented in Figure 9. Although all 7 specimens tested display similar characteristic nominal stress-strain behavior, some variations in measured effective stiffness and peak strength were observed due to stochastic flaws in the as-processed samples.

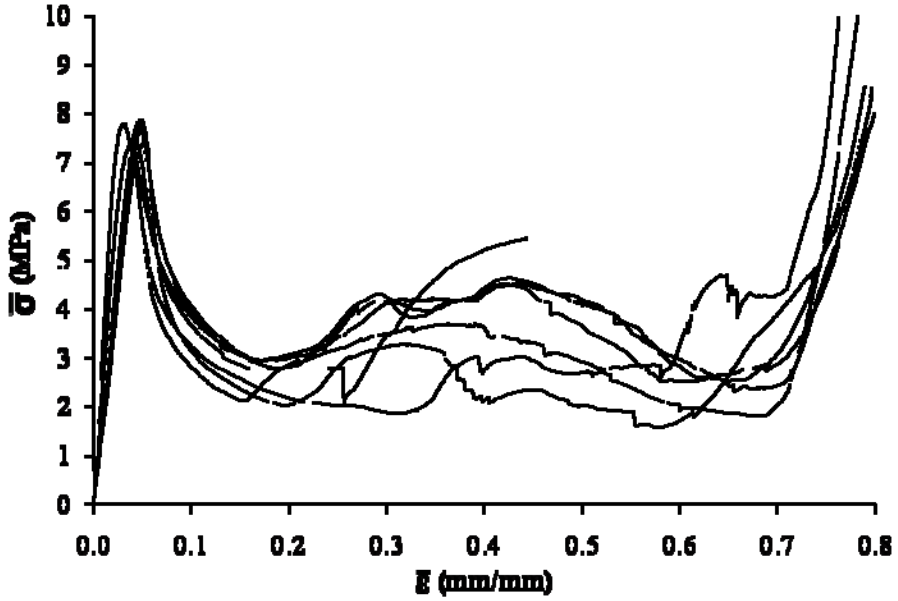

Figure 9: Optimized pyramidal core sandwich plates were tested in uniaxial out-of-plane compression and the nominal stress-strain response was measured

3.2.1 Peak Strength Calibration The average pyramidal core peak strength $\bar{\sigma}_{peak}$ obtained from Figure 9 is 7.6 MPa with a standard deviation of 0.4 MPa. In order to calibrate the analytical model in equation 8 with the experimental results, the bifurcation stress σ_{bif} was determined for the proposed strut geometry and parent material. Figure 10 represents the Shanley tangent method of iteratively evaluating the tangent modulus from the parent material stress-strain response to determine the buckling stress prescribed by strut geometry.

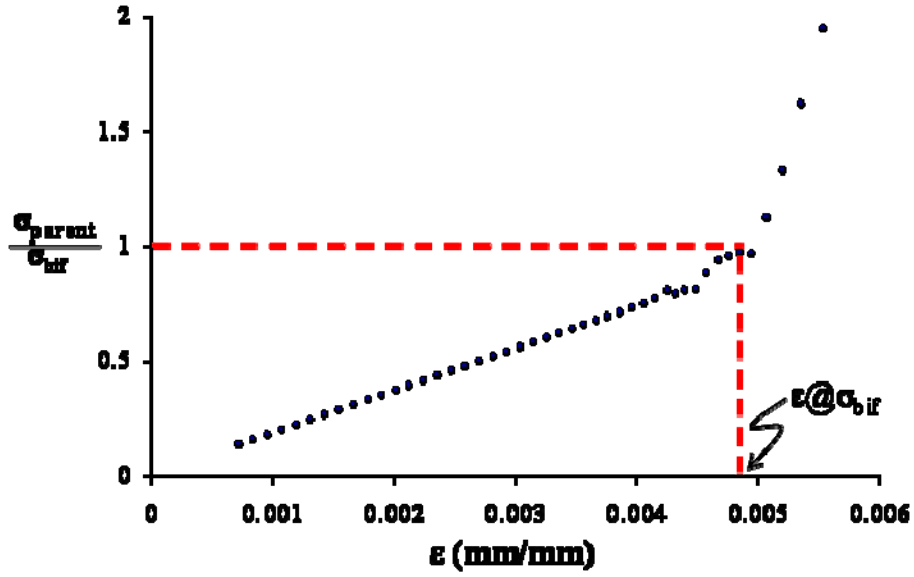

Figure 10: Bifurcation stress σ_{bif} is determined via the Shanley tangent method

Using this method, σ_{bif} is calculated to be 544.4 MPa at the strain where σ_{bif} equals σ_{parent}. From Figure 10 it is evident that this bifurcation stress occurs at the onset of non-linear stress-strain behavior for the parent material. This confirms that the use of parent material yield strength for optimization will produce a strength-to-weight optimized core. Using σ_{bif} in equation 8 along with the optimized core dimensions given in Table 1, $\bar{\sigma}_{peak}$ is calculated to be 8.0 MPa. Although this analytical prediction of $\bar{\sigma}_{peak}$ is consistently greater than the experimentally-measured value; Figure 9; the prediction is within one standard deviation of the experimental average. Thus, the model proposed in equation 8 is authenticated as a robust tool for predicting pyramidal core peak strength for the proposed collapse mode (minimal torsion).

3.2.2 Stiffness Calibration The average pyramidal core stiffness $\bar{E}$ obtained experimentally from Figure 9 is 214.4 MPa with a standard deviation of 55.5 MPa. Using the optimized core dimensions, core stiffness is predicted to be 537.8 MPa using equation 16. These results reveal that core stiffness is drastically over-predicted for the optimized core geometry. This discrepancy can be explained by investigating possible sources of strain measurement error during experimental testing. The predominate source of error is identified as settling of the structure that occurs due to minor manufacturing flaws such as facesheet rippling, minor variations in pyramid height, and imperfect braze joints. These factors all have a similar effect on strain data, as they would inflate strain measurements, thereby reducing the explicit observation of $\bar{E}$.

In order to investigate the proposed strain measurement errors; experiments were conducted on single pyramid plates. These experiments minimize the effects of facesheet rippling and varying core height because total deformation is isolated to a single cell. Figure 11 shows the nominal stress-strain response of a single unit cell specimen versus a multi-celled specimen.

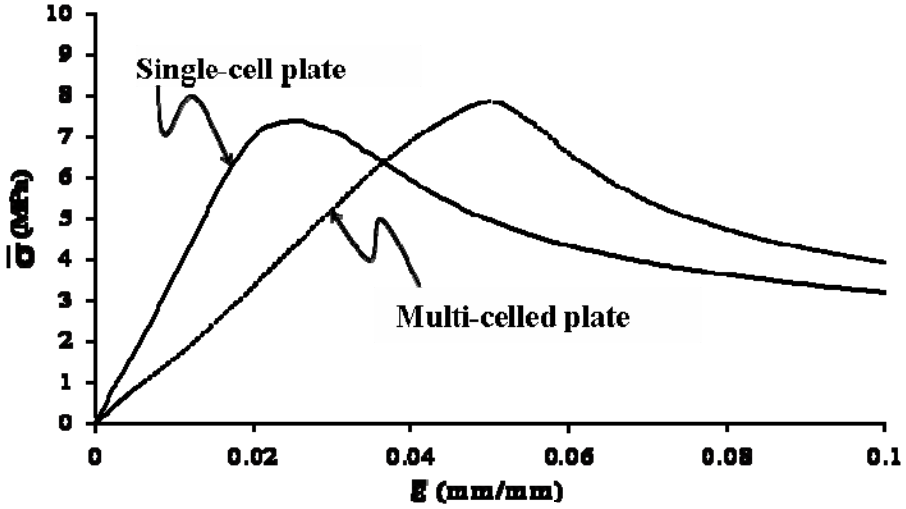

Figure 11: Both single pyramid and multi-celled specimens were tested in flatwise compression to verify the proposed measurement error of effective core stiffness $\overline{E}$

From visual inspection of Figure 11, it is evident that an improvement in measured core stiffness has been attained in the single unit cell experiments. Quantitatively, average measured core stiffness $\overline{E}$ is 362.1 MPa with a standard deviation of 6.0 MPa for the single unit cell experiments. Joint imperfections are believed to be the predominant source of measured deformation which is not accounted for in the analytical model of $\overline{E}$; equation 16. Joint anomalies such as porosity and thermal cracks are imperfections which have been identified in previous studies that account for the discrepancy between measured and predicted compressive core stiffness (7). Generally, modeling core stiffness requires that all joints be perfectly elastic and homogeneous. Since brazed joints cannot provide perfect joint properties, an improved core stiffness model accounting for joint deficiencies should be explored in future studies.

4. CONCLUSIONS

This study addresses many aspects of design and modeling of titanium pyramidal core sandwich plates. First, a manufacturing technique for fabricating cores from wrought material is outlined. Analytical models for peak strength and effective stiffness in compression are also ascertained. Next, a core optimization technique is implemented, and optimized sandwich plates are manufactured and tested in compression under quasi-static loading conditions. Compression results reveal that the peak strength model; equation 8; is a robust and accurate tool for depicting core performance. In addition, experimentally-measured stiffness is found to be significantly less than the analytical prediction. However, credible sources of reduced stiffness as well as improved techniques for measuring core deformation are presented. Finally, experimental findings confirm that the optimization technique implemented results in an optimized core. These results provide the Army with tools for design of pyramidal core sandwich structures to improve overall mobility and protection of future military vehicles.

5. REFERENCES

1. R. Hamilton, et. al. "Multiscale modeling for the prediction of casting defects investment cast aluminum alloys," Materials Science and Engineering A, **343**, (1-2), 290 (2003).
2. J. Zhou, P. Shrotriya, and W. Soboyejo. "On the deformation of aluminum lattice block structures: from struts to structures," Mechanics of Materials, **36**, (8), 723 (2004).
3. H. Wadley, N. Fleck, and A. Evans. "Fabrication & structural performance of periodic cellular sandwich structures," Composites Science & Technology, **63**, (16), 2331 (2003).
4. A. Evans, et al. "The topology design of multifunctional cellular metals," Progress in Materials Science, **46**, (3-4), 309 (2001).
5. M. Zupan, V. Deshpande, and N. Fleck. "The out-of-plane compressive behavior of woven-core sandwich plates," European Journal of Mechanics A/Solids, **23**, (3), 411 (2004).
6. ASTM Standard, "B265-03: Standard specification for titanium and titanium alloy strip, sheet, and plate," Annual Book of ASTM Standards, 2003.
7. K. Doherty, J. Tice, S. Szewczyk, and G. Gilde. "Titanium Brazing for Structures and Survivability," International Brazing and Soldering Conference Manuscript, (2006).
8. L. Gibson, and M. Ashby. Cellular Solids-Structure and Properties, Second edition. Cambridge University Press, 1998.
9. ASTM Standard, "C365-03: Standard test method for Flatwise Compressive Properties of Sandwich cores," Annual Book of ASTM Standards, 2003.

6. APPENDIX

Parameter	Dimension
Strut thickness, t	0.61 mm
Strut width, b	2 mm
Strut length, L	12 mm
Minor perforated sheet angle, α	70.529°
Major perforated sheet angle, β	109.471°
Joint width, ω	2.449 mm
Bend angle, Φ	90°
Interior angle, θ	35.264°
Core height, H	6.93 mm
Core base widths, X & Y	13.856 mm

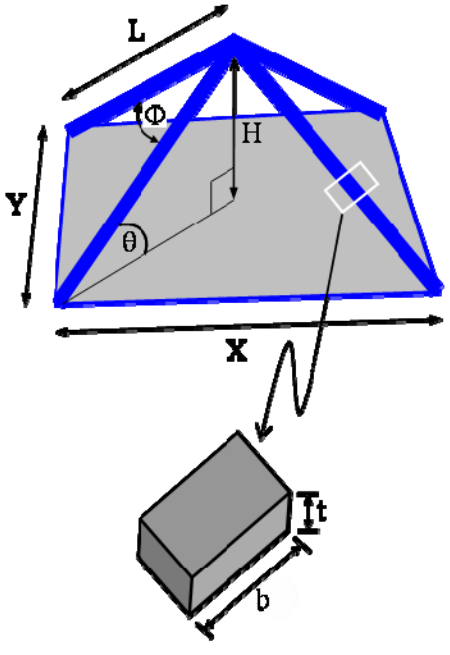

Table 1: All pertinent pyramidal core dimensions for an optimized core are heavily dependent on material selection; dimensions are shown here are for 0.61 mm thick CP-1

NO. OF
COPIES ORGANIZATION

1 (PDF ONLY) DEFENSE TECHNICAL INFORMATION CTR
DTIC OCA
8725 JOHN J KINGMAN RD
STE 0944
FORT BELVOIR VA 22060-6218

1 US ARMY RSRCH DEV & ENGRG CMD
SYSTEMS OF SYSTEMS INTEGRATION
AMSRD SS T
6000 6TH ST STE 100
FORT BELVOIR VA 22060-5608

1 DIRECTOR
US ARMY RESEARCH LAB
IMNE ALC IMS
2800 POWDER MILL RD
ADELPHI MD 20783-1197

3 DIRECTOR
US ARMY RESEARCH LAB
AMSRD ARL CI OK TL
2800 POWDER MILL RD
ADELPHI MD 20783-1197

ABERDEEN PROVING GROUND

1 DIR USARL
AMSRD ARL CI OK TP (BLDG 4600)

NO. OF COPIES ORGANIZATION

1 COMMANDER
NGIC
J CRIDER
W GSTATTENBAUER
2055 BOULDERS RD
CHARLOTTESVILLE VA 22901-5391

5 NAVAL SURFACE WARFARE CTR
U SORATHIA
C WILLIAMS CODE 6551
T BURTON CODE 667
R CRANE CODE 6553
R PETERSON CODE 2120
9500 MACARTHUR BLVD
WEST BETHESDA MD 20817

3 NAVAL RSCH LAB
B METZBOWER
D MICHEL
R KERANS
USSS OVERLOOK AVE SW
WASHINGTON DC 20373

2 THE BOEING CO
J CHILDRESS
N GERKEN
MS 84 69
PO BOX 359
SEATTLE WA 98124

1 SANDIA NATL LAB
TECH LBRY
PO BOX 5800
ALBUQUERQUE NM 87185-0307

1 DIRECTOR
LOS ALAMOS NATL LAB
G E CORT F663
TECH LBRY
PO BOX 1663
LOS ALAMOS NM 87545

1 AIR FORCE ARMAMENT LAB
AFATL DLJW
TECH LBRY
EGLIN AFB FL 32542

1 DEFENSE NUCLEAR AGCY
TECH LBRY
6801 TELEGRAPH RD
ALEXANDRIA VA 22192

NO. OF COPIES ORGANIZATION

3 COMMANDER
US ARMY TACOM
AMSRD TAR R
D TEMPLETON MS263
L P FRANKS MS 263
AMSTA TR D
M MAZZARA
6501 ELEVEN MILE RD
WARREN MI 48397-5000

2 PROJECT MGR
GROUND SYS INTEGRATION
SFAE GCSS W GSI
T DEAN
J ROWE
WARREN MI 48397-5000

3 COMMANDER
US ARMY RSCH OFC
D STEPP
J CHANG
W MULLINS
PO BOX 12211
RSCH TRIANGLE PARK NC
27709-2211

7 INST FOR ADVNCD TECH
W REINECKE
S BLESS
H FAIR
P SULLIVAN
T KIEHNE
D LITTLEFIELD
R SUBRAMANIAN
PO BOX 202797
AUSTIN TX 78720-2797

3 SOUTHWEST RSRCH INST
C ANDERSON
J RIEGEL
J WALKER
6220 CULEBRA RD
SAN ANTONIO TX 78238

2 UNIV OF DAYTON RSRCH INST
KLA14
N BRAR
A PIEKUTOWSKI
300 COLLEGE PARK
DAYTON OH 45469-0182

NO. OF
COPIES ORGANIZATION

3 GDLS
G TEAL
C OROURKE
C NIESE
38500 MOUND RD
STERLING HTS MI 48310-3200

1 OSD OUSD(A&T)/ODDR&E (W)
L SLOTER
1777 N KENT ST
STE 9030
ARLINGTON VA 22209

1 US MILITARY ACADEMY
DEPT OF MATH AND SCI
WEST POINT NY 10996-1786

4 DIRECTOR
DARPA
S WAX
A ALVING
L CHRISTODOULOU
D HONEY
3701 N FAIRFAX DR
ARLINGTON VA 22203-1714

1 UNIV OF DELAWARE
DEPT OF MECH ENGR
J GILLESPIE
201 SPENCER LAB
NEWARK DE 19716

2 MATERIAL TEST DIR
CSTE DTC WS MT
H W BENNET
R GRAJEDA
WSMR NM 88002

1 COMMANDER
US ARMY ARDEC
SMCAR AAE W
TECH LBRY
PICATINNY ARSENAL NJ 07806-5000

1 NAVAL WPNS CTR
TECH LBRY
CHINA LAKE CA 93555

1 NSWC DAHLGREN DIV
TECH LBRY
17320 DAHLGREN RD
DAHLGREN VA 22448

NO. OF
COPIES ORGANIZATION

2 NASA LANGLEY RSRCH CTR
AMSRD ARL VT
F BARTLETT JR MS266
G FARLEY MS 266
HAMPTON VA 23681-0001

8 UNIV OF MARYLAND
BALTIMORE COUNTY (UMBC)
DEPT OF MECH ENGR
M ZUPAN (5 CPS)
T FARQUHAR
W ZHU
D AROLA
1000 HILLTOP CIR
BALTIMORE MD 21250

ABERDEEN PROVING GROUND

39 DIR USARL
AMSRD ARL WM
J SMITH
AMSRD ARL WM MD
E CHIN
B CHEESEMAN
K DOHERTY (3 CPS)
J TICE (5 CPS)
S GHIORSE
J LASALVIA
J MONTGOMERY
J SANDS
C YEN
R DOOLEY
S WALSH
AMSRD ARL WM B
M ZOLTOSKI
AMSRD ARL WM MC
M MAHER
T JESSEN
R BRUCE
R REINSEL
AMSRD ARL WM MB
L BURTON
T BOGETTI
A YIOURNAS
AMSRD ARL WM MA
M VAN LANDINGHAM
R JENSEN
AMSRD ARL WM M
R DOWDING
J MCCAULEY
J BEATTY
S MCNIGHT

NO. OF
COPIES ORGANIZATION

AMSRD ARL WM TA
S SCHOENFELD
C HOPPEL
E HORWATH
C KRAUTHAUSER
N GNIAZDOWSKI
AMSRD ARL WM T
P BAKER
AMSRD ARL WM TC
R COATES

INTENTIONALLY LEFT BLANK.